Since January 2020 Elsevier has created a COVID-19 resource centre with free information in English and Mandarin on the novel coronavirus COVID-19. The COVID-19 resource centre is hosted on Elsevier Connect, the company's public news and information website.

Computers in Biology and Medicine 145 (2022) 105478

Contents lists available at ScienceDirect

Computers in Biology and Medicine

journal homepage: www.elsevier.com/locate/compbiomed

Interference of Chaga mushroom terpenoids with the attachment of SARS-CoV-2; *in silico* perspective

Wael M. Elshemey [a,*], Abdo A. Elfiky [b], Ibrahim M. Ibrahim [b], Alaa M. Elgohary [b]

[a] Physics Department, Faculty of Science, Islamic University of Madinah, Madinah, Saudi Arabia
[b] Biophysics Department, Faculty of Sciences, Cairo University, Giza, Egypt

ARTICLE INFO

Keywords:
COVID-19
HSPA5
GRP78
NAMD
MM-GBSA
Chaga terpenoids

ABSTRACT

Finding a potent inhibitor to the pandemic SARS-CoV-2 is indispensable nowadays. Currently, *in-silico* methods work as expeditious investigators to screen drugs for possible repurposing or design new ones. Targeting one of the possible SARS-CoV-2 attachment and entry receptors, Glucose-regulated protein 78 (GRP78), is an approach of major interest. Recently, GRP78 was reported as a recognized representative in recognition of the latest variants of SARS-CoV-2. In this work, molecular docking and molecular dynamics simulations were performed on the host cell receptor GRP78. With its many terpenoid compounds, Chaga mushroom was tested as a potential therapeutic against the SARS-CoV-2 receptor, GRP78. Results revealed low binding energies (high affinities) toward the GRP78 substrate-binding domain β (SBDβ) of Chaga mushroom terpenoids. Even the highly specific cyclic peptide Pep42, which selectively targeted GRP78 over cancer cells *in vivo,* showed lower binding affinity against GRP78 SBDβ compared to the binding affinities of terpenoids. These are auspicious results that need to be tested experimentally. Intriguingly, terpenoids work as a double sword as they can be used to interfere with VUI 202,012/01, 501.V2, and B.1.1.248 variants of SARS-CoV-2 spike recognition.

1. Introduction

SARS-CoV-2, which appeared in the 21st century, has caused many drastic changes in the fabric of the world [1]. COVID-19 pandemic is still producing health and economic consequences, while great efforts are spent on finding possible antivirals [2]. Many host-cell receptors are identified by the coronaviruses, including heparan sulfate proteoglycans, Aminopeptidase N, Angiotensin-Converting Enzyme 2 (ACE2), furin, O-Acetylated Sialic Acid, and the Glucose Regulated Protein 78 (GRP78) [1,3–9]. Directly after the entry of the virus, it kills the T lymphocyte cells, which leads to lymphopenia. Meanwhile, the inflammatory response activated via the virus also starts attacking the lymphocyte cells and leads to their apoptosis. Ultimately, when the viral particles have accumulated, some symptoms start to appear, such as destruction in the endothelial barrier, losing the capacity of oxygen diffusion, and in severe cases, the increase in inflammation caused by different cytokines can lead to death [10]. In addition, many studies have predicted the interaction between different molecules and the RBD of the spike protein [11–13]. Our main concern is targeting GRP78, accordingly, contradicting the SARS-CoV-2 entry.

GRP78, or binding immunoglobulin protein (BiP), is encoded by the heat shock protein A5 (*HSPA5*) gene and reside inside the endoplasmic reticulum (ER) of normal cells [14–16]. GRP78 functions as a chaperone protein that binds to unfolded proteins and directs them to the refolding or degradation machinery; hence it is described as the master of the unfolded protein response (UPR) mechanism [16]. Thus, stressed cells have elevated levels of GRP78 expression in order to overcome the massive number of unfolded proteins. In the dormant stable cell states, three transmembrane stress sensor proteins (residing in the ER)are bound to GRP78. These are the Activating transcription factor 6 (ATF6), protein kinase RNA-like endoplasmic reticulum kinase (PERK), and Inositol-requiring enzyme 1 (IRE1) [17,18]. When the stress signal sparks, the three proteins are released and become active in order to alleviate the stress inside the cell. Consequently, GRP78 is overexpressed and translocated to other cellular compartments, including the cell membrane, where the chaperone protein can carry out various functions [18–24]. Once exposed to the cell surface, GRP78 acts as a gate for pathogen recognition and entry [3,21,25–28]. We previously reported the possibility of recognizing SARS-CoV-2 spike by the cell-surface GRP78 and defined the spike region C480–C488 as the recognition site [3]. This recognition was validated experimentally by Lee et al., who identified the association of GRP78 with both human Angiotensin-converting enzyme 2 (ACE2) and SARS-CoV-2 spike protein

* Corresponding author.
E-mail address: welshemey@iu.edu.sa (W.M. Elshemey).

https://doi.org/10.1016/j.compbiomed.2022.105478
Received 16 January 2022; Received in revised form 23 March 2022; Accepted 30 March 2022
Available online 7 April 2022

List of abbreviations

ACE2	Angiotensin-Converting Enzyme 2
ADMET	Absorption, Distribution, Metabolism, Exceretion, and Toxicity
ATF6	Activating transcription factor 6
BBB	Blood Brain Barrier
BiP	binding immunoglobulin protein
CHARMM	Chemistry at Harvard Macromolecular Mechanics
CS-GRP78	cell-surface GRP78
EGCG	(−)-Epigallocatechin gallate
ER	endoplasmic reticulum
GRP78	Glucose-regulated protein 78
HSPA5	heat shock protein A5
IRE1	Inositol-requiring enzyme 1
MDS	Molecular Dynamic Simulation
MM-GBSA	Molecular Mechanics Generalized Born and Surface Area
NAMD	nanoscale molecular dynamics
PERK	protein kinase RNA-like endoplasmic reticulum kinase
RBD	receptor-binding domain
RMSD	Root Mean Square Deviation
RMSF	Root Mean Square Fluctuations
RoG	Radius of Gyration
SASA	surface Accessible Surface Area
SBDα	substrate-binding domain α
SBDβ	substrate-binding domain β
SDF	structure-data file
UFF	universal force field
UPR	unfolded protein response

[9].

Elevated levels of GRP78 were reported in COVID-19 patients [29]. Moreover, increased severity of COVID-19 (patient needs ICU or died) was reported in cancer patients compared to normal individuals [30]. A number of natural remedies were suggested to be important in fighting against COVID-19 [31–33]. Various naturally-derived compounds such as terpenoids were able to block the site of the cell-surface GRP78 (CS-GRP78) recognition, the receptor-binding domain β, and to compete for pathogen recognition [34,35]. Terpenoids from Chaga mushroom (*Inonotus obliquus*) were reportedly anti-cancerous effects [36,37]. Furthermore, we previously assessed the effectiveness of terpenoids in binding to SARS-CoV-2 spike protein, where twenty-eight terpenoid compounds were docked to the SARS-CoV-2 spike receptor-binding domain (RBD) [38]. Most of the tested terpenoids showed excellent binding affinities against the spike RBD (−5.6 down to −7.8 kcal/mol). At the same time, two of the terpenoids, betulinic acid, and inonotusane C, bonded near to the spike's ACE2 binding interface [38]. The rationale for testing the same group of terpenoids against GRP78 was that CS-GRP78 could recognize viral particles and hence might be a suitable target of the Mushroom terpenoids. Dual targeting of a viral protein and one of its host-cell receptors is promising to be tested against the mushroom terpenoids. It was not important to know the exact target of each of the investigated terpenoids. In fact, their combined affinity would make them a possible maestro in preventing infection.

In the present study, we predicted the binding potency of the same terpenoid compounds against the host-cell receptor GRP78 SBDβ, substrate-binding domain β, the same recognition site for CS-GRP78 by SARS-CoV-2 spike, juxtaposed with the peptide Pep42 and the (−)-Epigallocatechin gallate (EGCG) as positive controls. Other domains of GRP78 may also be available for terpenoids but are yet to be explored. The study was based on molecular docking and molecular dynamics simulation to mimic the terpenoids-GRP78 system in physiological conditions. These computational methods successfully suggested new drug candidates against COVID-19 [39–41]. After that, Molecular Mechanics Generalized Born and Surface Area (MM-GBSA) for the best two complexes (Oleanolic acid and Inonotsulide A) in addition to the residual contribution to the binding was calculated using MMPBSA.py implemented in AmberTools 17 [42].

2. Materials and methods

2.1. Structure retrieval

The structures of the terpenoid compounds (twenty-eight) were retrieved from the PubChem database [43]. Most of the terpenoids were found in the 3D structure-data files (SDF) on PubChem, so it was used to build the docking study's input files (PDBQT) utilizing AutoDock Tools software [44]. Unfortunately, few compounds were available on the PubChem as 2D, therefore we generated the 3D structures using Avogadro software and optimized the geometry using the steepest descent algorithm with the universal force field (UFF) of Avogadro [45,46].

On the other hand, the structure of the cyclic peptide Pep42 was built by comparative modeling from its amino acid sequence (CTVALPGGYVRVC) with the aid of the I-TASSER web server (https://zhanggroup.org/I-TASSER/, accessed on December 6, 2021) [25,47,48]. First, the cyclic peptide structure was constructed by forming the S–S bond between C1 and C13 using Avogadro software. Then, Molecular Dynamics Simulation (MDS) for 200 ns was performed on the cyclic peptide using CHARMM 36 force field in the nanoscale molecular dynamics (NAMD) software [49,50]. Cluster analysis was performed through Maestro software on the cyclic peptide trajectories. Finally, four main clusters were extracted to get representative conformations for the Pep42 to be used in the docking experiments [51].

2.2. Protein preparation

GRP78 structure (PDB ID: 5E84) was downloaded from the protein data bank (PDB) [52]. It exhibited the wild-type open conformation of GRP78 since other structures such as 6HAB, 5F0X, 3LDQ, and 6ZYH were either in the closed conformation or missing some domains [52,53]. The structure was then prepared for the docking study by removing water molecules and ligands while missing Hydrogen atoms were added with the help of PyMOL software [54].

2.3. Molecular dynamics, docking, and MM-GBSA calculations

The different conformations of GRP78 after 50 ns MDS run were used in the docking experiments. As reported before, four different conformations of the protein resembled the four most popular clusters of GRP78 trajectories. The protein's representative conformations were taken using Chimera software at 17.8, 26.2, 31.8, and 37.8 ns. [55]. The Pep42 cyclic peptide (selected conformations after MDS), EGCG, and the 28 terpenoids were tested against the four GRP78 conformations. AutoDock Vina software was used in the docking study, while AutoDock Tools and PyMOL were employed to generate the input files and analyze the output files [44,56]. All of the docking experiments followed a flexible ligand in a flexible active site protocol. The grid boxes were chosen to be of size 48 × 48 × 56 $Å^3$ centered at 30, 52, −24 Å (minor differences existed between the four different conformations of GRP78) with a default grid spacing of 0.375 Å. The searching box covered all of the active residues (I426, T428, V429, V432, T434, F451, S452, V457, and I459) [17,57].

For further analysis, the docking complexes were examined using the discovery studio visualizer software [58]. First, data were tabulated and

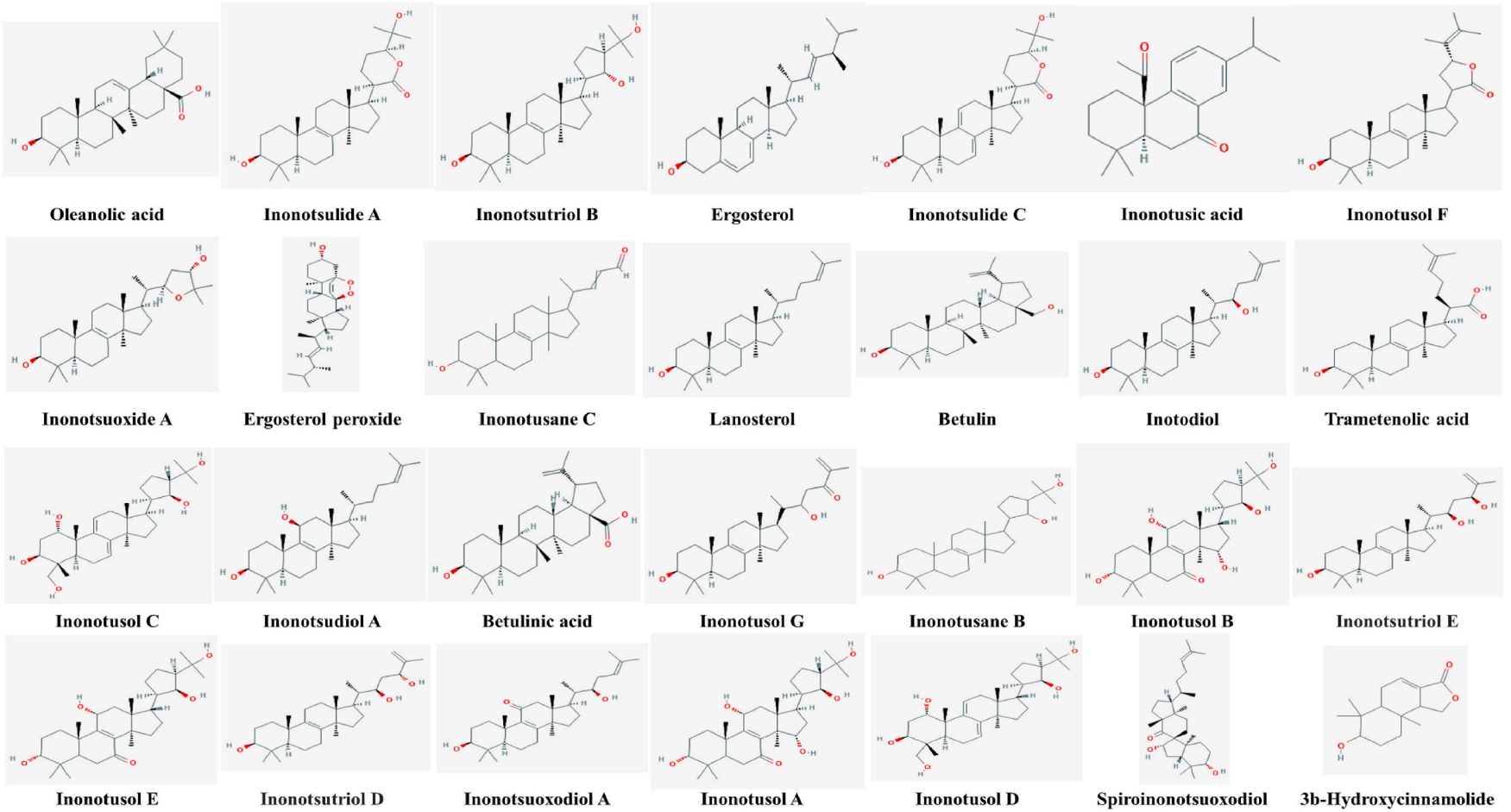

Fig. 1. 2D structures of the terpenoids ranked according to their binding affinities to GRP78 RBDβ.

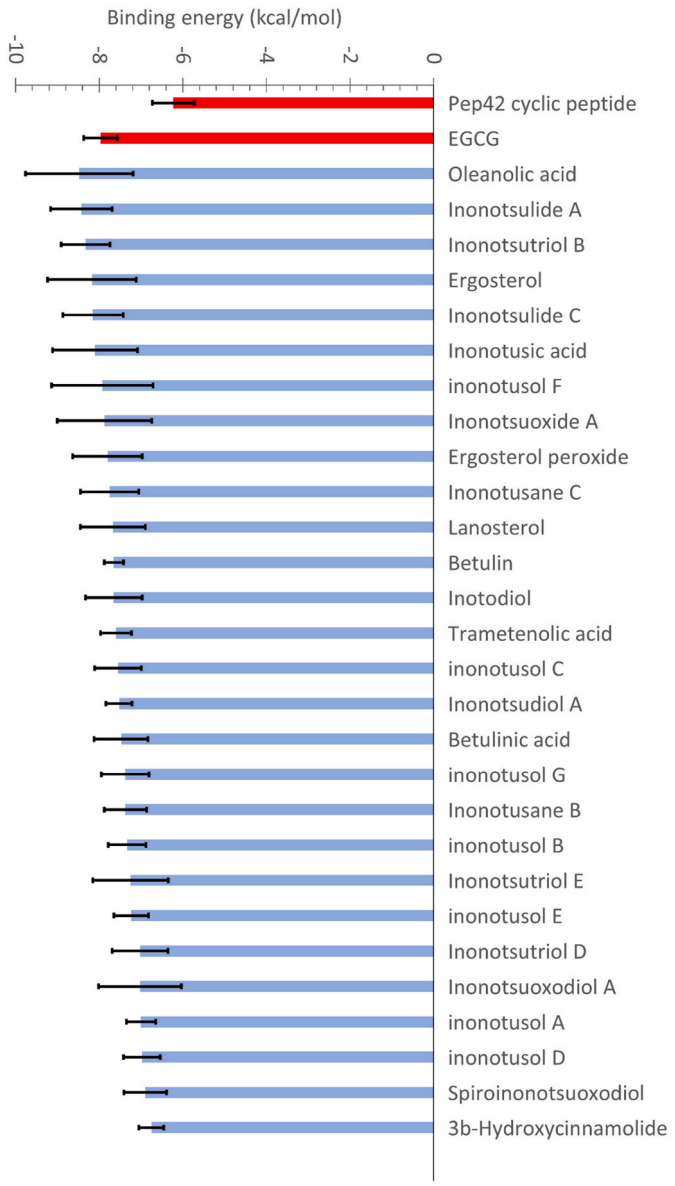

Fig. 2. The average binding energy (in kcal/mol) was calculated using AutoDock Vina software for docking the 28 terpenoid compounds against the four different conformations of GRP78 SBDβ. The peptide Pep42 and EGCG (red columns) are positive controls due to their specificity in binding HSPA5. (For interpretation of the references to color in this figure legend, the reader is referred to the Web version of this article.)

graphically presented through PyMOL and Discovery studio visualizer software [54]. Next, the best two compounds (Oleanolic acid and Inonotsulide A) complexes with GRP78 were subjected to 50 ns MDS run using the same protocol. This was followed by calculating the Molecular Mechanics Generalized Born and Surface Area (MM-GBSA) for the complexes in addition to the residual contribution to the binding [59]. Finally, the binding free energy differences were decomposed to its elements. The whole trajectory with a stride of 1 was used in the calculation of binding energy, and the method of generalized born (igb) was set to 5. MM-GBSA approach is depicted in eq. (1)

$$\Delta G = < Gcomplex - Greceptor - Gligand > \quad \text{Equation 1}$$

where $< >$ represents the average of the enclosed free energies of complex, receptor, and ligand over the frames used in the calculation. Different energy terms can be calculated following the equations from 2 to 6.

$$\Delta Gbinding = \Delta H - T\Delta S \quad \text{Equation 2}$$

$$\Delta H = \Delta Egas + \Delta Esol \quad \text{Equation 3}$$

$$\Delta Egas = \Delta Eele + \Delta EvdW \quad \text{Equation 4}$$

$$\Delta Esolv = EGB + ESA \quad \text{Equation 5}$$

$$ESA = \gamma.SASA \quad \text{Equation 6}$$

where ΔH is the enthalpy which can be calculated from gas-phase energy (E_{gas}) and solvation-free energy (E_{sol}). TΔS is the entropy contribution to the free binding energy, and it was not calculated because we want to compare the relative binding free energies. E_{gas} is composed of electrostatic and van der Waals terms; Eele, EvdW, respectively. The polar solvation energy (E_{GB}) and nonpolar solvation energy (E_{SA}) are used to calculate the E_{sol} [60,61].

2.4. ADMET properties calculation

pkCSM webserver was used to find the compound's druggability according to Lipinski's rule of five and to predict the Absorption, Distribution, Metabolism, Excretion, and Toxicity (ADMET) properties [62].

3. Results

Fig. 1 demonstrates the 2D structures of the terpenoids ranked according to their average binding affinities against GRP78 SBDβ from the top left (best compound) to the right bottom (worst in binding). Each terpenoid molecule was docked to the four different conformations of the GRP78 using AutoDock Vina.

3.1. Terpenoids binding energies against GRP78 SBDβ

Fig. 2 represents the average binding energies of the terpenoid compounds against the four different conformations of GRP78 (colored columns), compared to Pep42, and (−)-Epigallocatechin gallate (EGCG) as positive controls (red columns), while the error bars represent the standard deviation (SD) [63]. Surprisingly, all of the twenty-eight terpenoid compounds (blue columns) exhibit lower (better) binding affinities to the GRP78 SBDβ compared to Pep42, yet still in the same range as EGCG. The average binding energy values ranged from −8.48 ± 1.29 kcal/mol (Oleanolic acid) to −6.75 ± 0.30 kcal/mol (3b-Hydroxycinnamolide).

Table 1 shows the interactions established upon docking of the 28 terpenoids against GRP78 substrate-binding domain β, where the number and type of the interactions are listed. The selected complexes are ranked according to the average binding affinity as in Figs. 1 and 2. The complex selection was based on the binding affinity values, where the complex with binding affinity close to that of the mean value was selected for the analysis. The selected complexes were examined using the Discovery studio visualizer to analyze the data further.

Some complexes are represented graphically in Fig. 3. Fig. 3B depicts betulinic acid, and inonotusane C docked into the SBDβ of GRP78 to quantify their binding behavior and compare it to a previous study [38] where it is tightly bound to the spike of SARS-CoV-2 (Table 1).

3.2. Molecular dynamic simulations and binding free energy calculations for the best two complexes

Molecular dynamics simulations (50 ns) for the best two complexes (Oleanolic acid and Inonotsulide A) were performed using NAMD software, then MM-GBSA was calculated using amber tools. In Table 2, the residuals' contribution to GRP78 binding of the best two compounds

Table 1
The interactions were established on selected ligand-GRP78 complexes based on binding affinity values. Bold residues are the most repeated interactions in most ligands.

	H-bonding		Hydrophobic interaction		π-interaction	
Ligand	Number	Amino acids involved from GRP78	Number	Amino acids involved from GRP78	Number	Amino acids involved from GRP78
Pep42	3	Q449(2), Q492	2	I450 and V453	2	I426 and F451
EGCG	1	E427	5	I426, F451, I459(2), and K460	1	F451
Oleanolic acid			6	I426(2), **F451(2)**, and **I459(2)**	1	F451
Inonotsulide A	1	I450	7	**V429**, I450, **F451(2)**, **V453(2)**, and **I459**		
Inonotsutriol B	1	E427	7	**V429(3)**, **F451(2)**, and **V453(2)**	1	F451
Ergosterol			7	**V429(3)**, **F451**, and **V453(3)**	1	F451
Inonotsulide C			5	**V429**, **F451**, **V453(2)**, and **I459**		
Inonotusic acid	1	T458	4	**V429(2)**, **F451**, and **V453**	3	V429, F451(2)
Inonotusol F			6	**V429**, **F451(2)**, **V453(2)**, and V457		
Inonotsuoxide A			4	**F451**, **I459**, K460, and V495	1	F451
Ergosterol peroxide			7	I426(2), **F451(2)**, **I459**, K460, and V495	1	F451
Inonotusane C			9	I426(2), **V429**, **F451(5)**, and V495	1	F451
Lanosterol			12	I426, **F451(5)**, **I459(3)**, K460(2), and Y462		
Betulin			11	**V429(2)**, **F451**, **V453(5)**, V457, and **I459(2)**	1	F451
Inotodiol			9	I426, **F451(2)**, **I459(2)**, K460, V495(2), and F497		
Trametenolic acid	1	E427	8	I426, **F451**, **I459(2)**, K460, V495(2), and F497	1	F451
Inonotusol C	2	I450 and K460	7	I426 (2), **F451(2)**, **I459**, and K460(2)		
Inonotsudiol A			9	**V429(3)**, **F451(3)**, and **V453(3)**		
Betulinic acid	2	E427 and I450	4	**I426**, **F451**, andI459**(2)**		
Inonotusol G			5	**F451**, **V453(2)**, V457, and K460		
Inonotusane B			11	**V429(2)**, **F451(3)**, **V453(2)**, V457, and **I459 (3)**		
Inonotusol B			7	I426, **F451(3)**, **V453**, and **I459(2)**		
Inonotsutriol E			7	**V429**, **F451**, **V453(3)**, V457, and **I459**	1	F451
Inonotusol E	2	Q449 and T458	6	**V429(2)**, I450, **F451**, **V453**, and V457	1	F451
Inonotsutriol D			6	**V429**, **F451(2)**, **V453(2)**, and **I459**		
Inonotsuoxodiol A	2	K460(2)	7	**V429**, **F451(4)**, and **I459(2)**	1	F451
Inonotusol A	3	E427(2) and G430	6	**V429(2)**, **F451(2)**, and **V453(2)**		
Inonotusol D	2	E427 and T428	7	I426(2), **F451(2)**, **I459(2)**, and K460		
Spiroinonotsuoxodiol			9	I426, **F451(2)**, **V453(2)**, V457, and **I459(3)**		
3b-Hydroxycinnamolide	1	T458	4	I426, **F451(2)**, **V453**	1	F451

(Oleanolic acid and Inonotsulide A) are listed.

Fig. 4 supports the previous results as the two complexes were equilibrated for 50 ns (flattened RMSD after about 8 ns (Fig. 4A)). Additionally, the RoG and the surface Accessible Surface Area (SASA) were stable during the simulation period. The (GRP78-Oleanolic acid complex (orange line) showed more stable RoG values compared to GRP78-Inonotsulide A complex (gray line). Additionally, the former complex possessed a less deviated RMSD profile (about 6 Å) compared to the latter complex (RMSD around 8 Å). This might indicate the stability of the first complex relative to the other one. Fig. 4B shows the per-residue Root Mean Square Fluctuations (RMSF) in Å for the apo-GRP78 (blue line) and the two complexes (GRP78-Oleanolic acid and GRP78-Inonotsulide A). The apo-GRP78 and the GRP78-Oleanolic acid complex were almost the same, showing fluctuations (RMSF < 8 Å) at the SBDα (residues 565–600) and the N and C termini. On the other hand, GRP78-Inonotsulide A complex showed higher fluctuations in SBDα (residues 565–600) and SBDβ (residues 428–491) and even in the nucleotide-binding domain (residues 133–138) of the GRP78. This reflected the complex's stability in the case of Oleanolic acid compared to GRP78-Inonotsulide A complex.

3.3. ADMET properties of Chaga mushroom terpenoids

Table 3 shows the properties of each compound and whether they agree with the Lipiniski's rules of five (green) or not (red). Nearly all of the studied terpenoids are druggable according to the rule of five except for the values of LogP of Inonotusol G, and Inonotusic acid compounds (shown in red in Table 3). Additionally, the pkCSM webserver was used to check the ADMET properties as tabulated in Table 4.

4. Discussion

We previously reported *in silico* the *Inonotus obliquus* terpenoids' effectiveness (Chaga mushrooms) in binding the receptor-binding domain of SARS-CoV-2 spike protein [38]. Most of the terpenoid compounds were reported to be tightly bound to the spike protein at the receptor-binding domain at the ACE2 binding surface. At the same time, betulinic acid (−7.5 kcal/mol) and inonotusane C (−7.4 kcal/mol) were the best two compounds in binding the spike. On the other hand, Beta glycan, betulinic acid, and galactomannan show high affinity against the S1 (−7.4 to −8.6 kcal/mol) of the spike as reported in another prediction study [64].

According to our previous work, the 50 ns MDS was enough to equilibrate the GRP78 system [35]. Meanwhile, the cyclic peptide Pep42 was simulated for 200 ns MDS at the same physiological conditions of salt, water, and temperature. The protein (GRP78) and the cyclic peptide (Pep42) systems were equilibrated during the first 20 ns of the simulation as reflected from the Root Mean Square Deviation (RMSD) and the Radius of Gyration (RoG) curves (in Å) versus the simulation time (ns) shown in the Supplementary Fig. S1. Pep42 was proved to be the distinctive docking element of GRP78 SBDβ [65,66], giving average binding energy of -6.23 ± 0.50 kcal/mol, while for EGCG, it gave a value of -7.97 ± 0.40 kcal/mol.

Up on docking, the main types of established interactions were; the formation of H-bonds and hydrophobic contacts with some π-sigma, π-alkyl, and π-π stacked interactions in some complexes as shown in Table 1, where the most repeated interactions are in bold. The F451 residue in GRP78 was the most frequent in forming contacts (hydrophobic) with terpenoids with a total of 74 interactions (π-sigma and π-alkyl hydrophobic contacts). The V453, I459, V429, and I426 residues

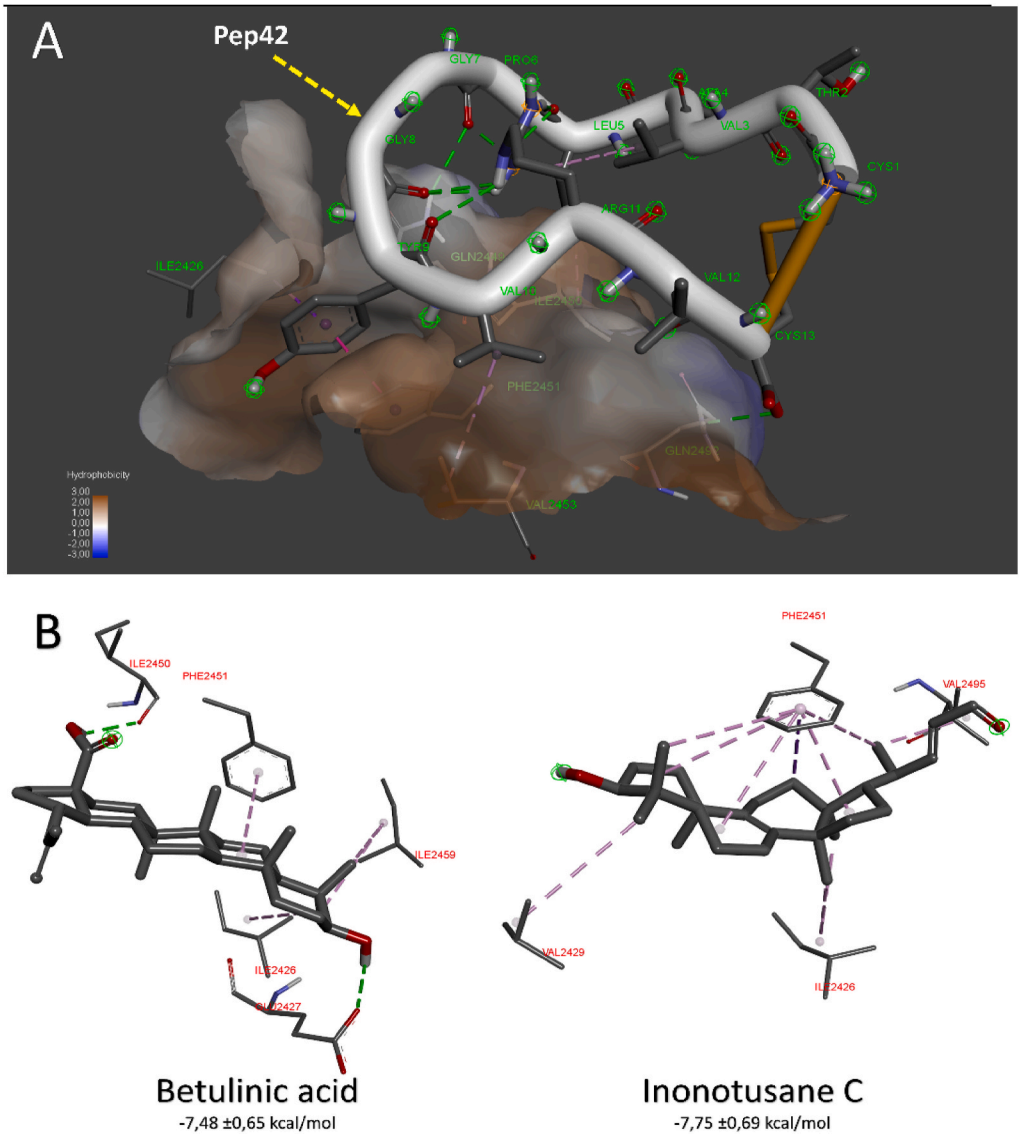

Fig. 3. A) The interaction pattern of Pep42 cyclic peptide (white cartoon and sticks) with GRP78 SBDβ (wires). The protein surface is calculated and represented by the hydrophobicity according to the color scheme at the figure's lower-left corner. (B) The interaction pattern of Betulinic acid and Inonotsane C (sticks) against GRP78 SBDβ (wires). The H-bonds and hydrophobic contacts are depicted by dashed-green lines and dashed-iris lines, respectively. (For interpretation of the references to color in this figure legend, the reader is referred to the Web version of this article.)

Table 2
The MM-GBSA calculations for the best two complexes after 50 ns MDS. Red-colored residues represent the residues that have a negative contribution to binding (positive binding energies). The average binding free energies and their terms are shown at the bottom of the table for each complex with its standard deviations.

COMPLEX	*GRP78* - Oleanolic acid *complex*		*GRP78* - Inonotsulide A *complex*	
RESIDUAL CONTRIBUTION TO BINDING	*Residue*	*Binding energy (kcal/mol)*	*Residue*	*Binding energy (kcal/mol)*
	I459	*−1.47*	*R488*	*−1.21*
	V457	*−1.43*	*I483*	*−0.72*
	F451	*−1.35*	*V453*	*−0.68*
	I426	*−1.26*	*K460*	*−0.58*
	V429	*−1.01*	*I493*	*−0.40*
	V453	*−0.98*	*T458*	*−0.37*
	Q449	*−0.77*	*I459*	*−0.34*
	T428	*−0.58*	*V490*	*−0.30*
	V495	*−0.47*	*V457*	*−0.29*
	T477	*−0.26*	*A486*	*−0.26*
	T456	*−0.25*	*P484*	*−0.24*
	S448	*−0.25*	*P487*	*−0.21*
	G425	*−0.19*	*P491*	*−0.20*
	T458	*−0.16*	*Q492*	*−0.19*
	Q492	*−0.16*	*I520*	*−0.19*
	F478	*+0.21*	*I522*	*−0.18*
	G454	*+0.24*	*E427*	*+0.52*
	E427	*+1.12*	*D511*	*+0.73*
ΔE_{VDW} *(kcal/mol)*	*−31.05* ± 4.8		*−25.55* ± 13.2	
ΔE_{ELE} *(kcal/mol)*	*−5.13* ± 4.9		*−3.48* ± 6.5	
ΔG_{GB} *(kcal/mol)*	*18.07* ± 4.7		*16.06* ± 7.9	
ΔG_{SA} *(kcal/mol)*	*−4.39* ± 0.6		*−3.54* ± 1.8	
ΔG GAS (kcal/mol)	*−36.19* ± *5.9*		*−29.03* ± *14.7*	
ΔG SOLV (kcal/mol)	*13.68* ± *4.6*		*12.51* ± *6.8*	
ΔG TOTAL (kcal/mol)	*−22.51* ± *4.7*		*−16.51* ± *10.4*	

ΔE_{VDW} Van Der Waal's potential energy contribution, $\Delta E_{ELE,}$ Electrostatic potential energy contribution, ΔG_{GB} Generalized Bohrn binding energy contribution, ΔG_{SA} Surface Area binding energy contribution, *ΔG GAS,* Gas-phase binding energy contribution *ΔG SOLV* solvation binding energy contribution, *ΔG TOTAL* total binding energy.

formed 37, 34, 27, and 19 hydrophobic contacts with terpenoids, respectively. These hydrophobic patches of the substrate-binding domain β of GRP78 were the docking platform of the unfolded proteins in stressed cells [25,57].

On the other hand, Pep42 formed three H-bonds with Q449(2) and Q492, and four hydrophobic contacts with I450 & V453 (Alkyl contacts), I426 (π-sigma) and F451 (π-π stacked) of GRP78 (Fig. 3A). This is in excellent agreement with previous *in vivo* studies, where Pep42 was reported to selectively recognize and bind GRP78 over cancer cells [65,66]. Interestingly, the V453 residue, which resembles the substrate-binding defective mutant of GRP78, is reported here to bind to the Pep42 and 17 terpenoid compounds against GRP78. V453 was described as a crucial residue in spike and ACE2 recognition of GRP78 [9]. Whereas EGCG formed one H-bond to E427, one π-π stacking with F451, one π-sigma interaction with I459, two π-Alkyl interactions with F451 & K460, and two Alkyl interactions with I426 & I459.

Inonotusane C formed ten hydrophobic contacts (dashed-gray lines) with GRP78 residues I426(2), V429, F451(6), and V495. In comparison, betulinic acid interacted with both H-bonds (dashed-green lines) of E427 and I450 and formed four hydrophobic contacts (I426, F451, and I459(2)) with GRP78. It seems that F451 is very important in recognizing Inonotusane C by GRP78. It was involved in 6 hydrophobic interactions with almost every part of the molecule. Hydrophobic interactions were also a landmark of terpenoids interactions with SARS-CoV-2 spike (three in the case of inonotusane C and four in the case of betulinic acid), where K458 and Y473 were the most reported residues from the spike that formed these hydrophobic contacts with terpenoids [38].

The residues from GRP78 SBDβ, defined as the docking platform of the substrates I426, T428, V429, V432, T434, F451, S452, V457, and I459, are shown in bold and underlined in Table 2. For the GRP78-Oleanolic acid complex, I426, V429, V457, and I459 were the main contributors to binding (−1.26, −1.01, −1.43, and −1.47 kcal/mol, respectively), while for the GRP78-Inonotsulide A complex, R488 was the main contributor (−1.21 kcal/mol). The contribution of the substrate-binding site (bold and underlined) of GRP78 in the binding of Oleanolic acid to the protein is clear from Table 2 (−7.1 kcal/mol). In comparison, a lower contribution of these residues was reported in the case of the GRP78-Inonotsulide A complex (−0.63 kcal/mol). E427 (red-colored) negatively contributed to binding (having positive energy difference) in both complexes (+1.12 and + 0.52 kcal/mol for Oleanolic acid and Inonotsulide A, respectively). F478, G454, and D511 showed negative contributions to the binding. The total binding energy for the Oleanolic acid was lower (−22.51 kcal/mol) than for Inonotsulide A (−16.51 kcal/mol); hence Oleanolic acid was the best-suggested compound that could bind to GRP78 SBDβ.

According to Lipinski's rule of five, a compound is considered to be druggable if the number of hydron bond acceptors and donors is less than or equal to 10 and 5, respectively, its solubility (LogP) $\leq$ 5 and its molecular weight $\leq$500 Da [62,67].

For the ADMET properties, Table 4 shows the prediction of the pkCSM webserver. The absorption of the compounds can be predicted (according to Table 4) through three values (water solubility in log(mol/L), Caco2 permeability, and intestinal absorption). Compounds with more negative water solubility values, Caco2 permeability >0.9, and intestinal absorption >30% indicate that the server predicted them as soluble. Nearly all compounds achieved good Caco2 permeability and intestinal absorption values, and all compounds had a negative value less than −3.02 log mol/L. The next prediction is for the distribution of the terpenoids, which can be known through the fraction of compounds that are not bound to serum proteins and Blood-Brain Barrier (BBB) permeability. The higher the unbound fraction and the more negative the values of BBB permeability indicate a good distribution. Inhibitors of Cytochrome P450 can activate the drug metabolism and, therefore, be removed from the market. The compounds were used to predict whether they were inhibitors of different isoforms (CYP1A2, CYP2C19, CYP2C9,

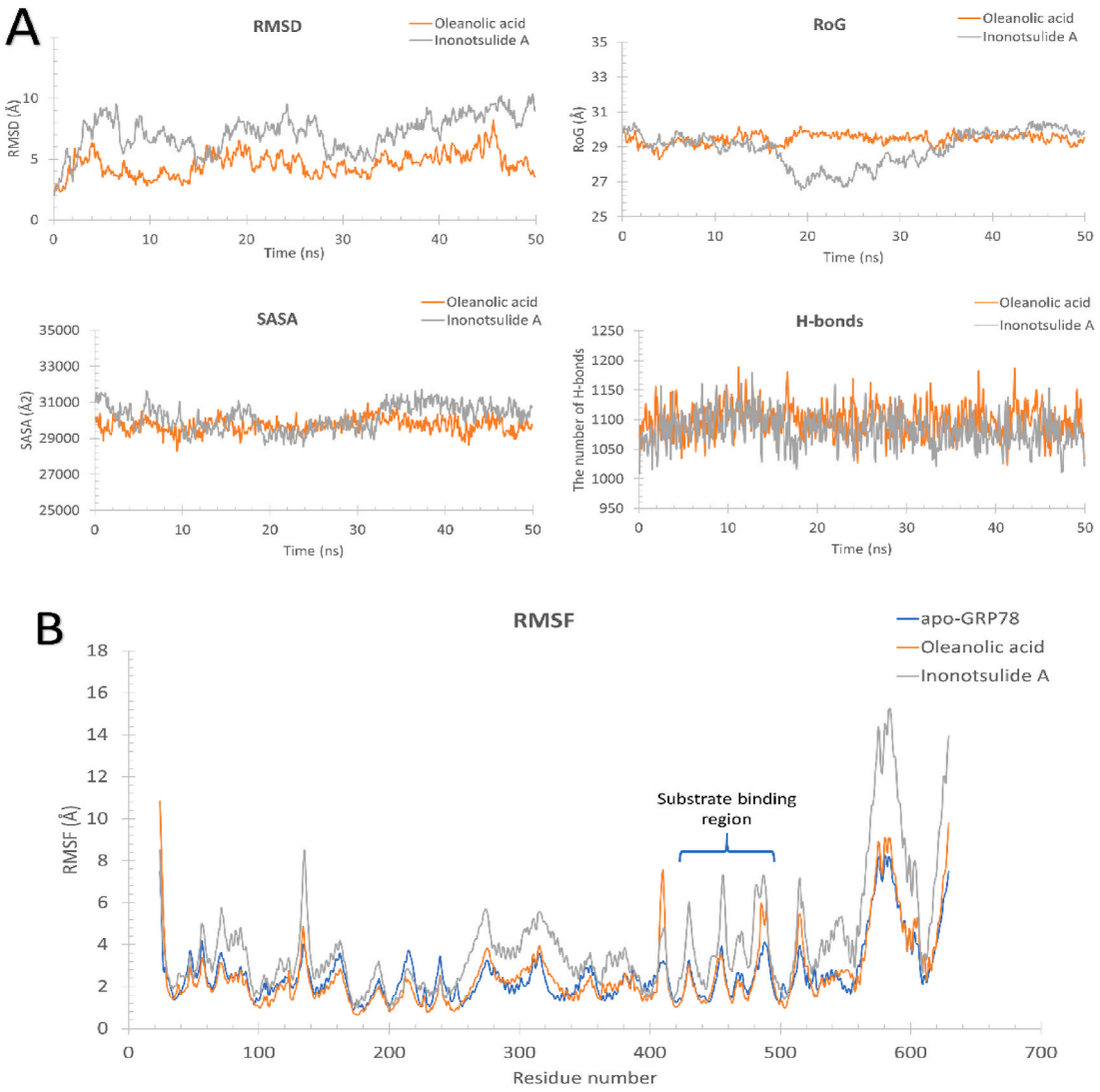

Fig. 4. (A) Root mean square deviation (RMSD) in Å and Radius of Gyration (RoG) in Å, Surface Accessible Scheme 2 and number of H-bonds versus time in ns for the MD simulation of GRP78-Oleanolic acid (orange) and GRP78-Inonotsulide A (gray) complexes. (B) Root Mean Square Fluctuations (RMSF) versus residue number of apo-GRP78 (blue), GRP78- Oleanolic acid (orange), and GRP78-Inonotsulide A (gray) complexes. (For interpretation of the references to color in this figure legend, the reader is referred to the Web version of this article.)

Table 3
Lipinski's rule of five for the terpenoids studied in this work. Green numbers indicate that the value agrees with the rule of five. Red numbers indicate that the value is higher than the threshold.

Compounds names	Number of H-donors	number of H-acceptors	LogP	Molecular weight
Inonotsutriol D	3	3	1.58314	411.351
Inonotsutriol B	3	3	0.91655	411.351
Inonotsuoxodiol A	2	3	1.24775	410.343
Inonotsuoxide A	2	3	1.40515	410.343
Inonotsulide C	2	4	0.51276	426.342
Inonotsulide A	2	4	0.51276	426.342
Inonotsudiol A	2	2	1.75994	394.344
Ergosterol peroxide	1	3	1.22716	385.313
Ergosterol	1	1	1.93674	353.315
Betulinic acid	2	2	1.35196	410.343
Betulin	2	2	1.67865	394.344
3b Hydroxycinnamolide	1	3	0.29938	229.17
Trametenolic acid	2	2	1.43325	410.343
Spiroinonotsuoxodiol	2	3	1.16646	410.343
Oleanolic acid	2	2	1.27067	410.343
Lanosterol	1	1	1.93674	377.337
Inotodiol	2	2	1.75994	394.344
Inonotusol G	2	3	6.33366	456.711
Inonotusol F	1	3	1.43744	421.346
Inonotusol E	4	5	0.22756	444.357
Inonotusol D	5	5	0.56295	445.365
Inonotusol C	5	5	0.56295	445.365
Inonotusol B	5	6	0.05076	461.364
Inonotusol A	5	6	0.05076	461.364
Inonotusic acid	0	2	5.0495	312.453
Inonotusane C	1	1	1.57407	357.303
Inonotusane B	3	3	0.91655	411.351
Inonotsutriol E	3	3	1.58314	411.351

CYP2D6, and CYP3A4). All compounds were predicted not to inhibit the last three isoforms, and only Inonotusic acid was predicted to be an inhibitor of CYP1A2 and CYP2C19. The model predicts whether a compound is a renal organic cation transporter 2 substrates for excretion. Since interaction with this transporter helps in the clearance of the compound and may produce adverse interactions, negative values are considered good. Only one compound (3b Hydroxycinnamolide) showed a positive prediction. Finally, toxicity is predicted through four indicators. Ames toxicity is a test that indicates whether the compound is a carcinogen. Inhibition of hERG I/II is the principal cause of fatal ventricular arrhythmia and has resulted in the withdrawal of many substances. As its name implies, hepatotoxicity indicates whether the compound may disrupt the liver's normal function. None of the studied terpenoids was predicted to have a carcinogenic effect or act as an inhibitor for hERG I. On the other hand, three compounds (Ergosterol peroxide, Ergosterol, and Lanosterol) were predicted to be inhibitors of hERG II. Five compounds (Trametenolic acid, Oleanolic acid, inonotusol E, inonotusol D, and inonotusol C) were predicted to cause hepatotoxicity to the liver.

Overall, most compounds showed excellent absorption, metabolism and excretion, good toxicity, and moderate distribution prediction, and most of them were considered druggable according to Lipinski's rule of five.

Targeting the cell-surface GRP78 is safe as this protein functions inside the ER as a chaperone. Therefore, we think that the administration of Chaga mushroom terpenoids would be safe with minimal or no side effects, but yet to be verified experimentally. The recognition of SARS-CoV-2 spike by the cell-surface GRP78 became significantly evident in the latest virus variants, the UK (VOC-202012/01), the South African (501.V2), and the Brazilian (B.1.1.248 lineage) in addition to Omicron variants [68–70]. Three potential mutations in the SARS-CoV-2 spike were reported in these new variants of the virus (K417 N, E484K, and N501Y). The second mutation was located in the GRP78 recognition site (C480–C488 of the spike), previously reported by our group [3]. Additionally, Khater and Nassar noted that neutralizing antibodies alone against ACE2 is not enough in fighting against delta and delta-plus variants of SARS-CoV-2. They suggested that inhibitors are essential in blocking GRP78-spike recognition [71]. Thus, the present study suggests that terpenoids are robust candidates in influencing the spread of SARS-CoV-2 new variants. Hence, Chaga mushroom's terpenoids might be used as prophylactic agents for high-risk personals such as elders, the front-line medical staff, and diabetic & cancer patients.

5. Conclusion

Terpenoids, found in the Chaga mushroom, have been reported to bind to the spike of SARS-CoV-2 with acceptable binding affinity. Furthermore, in the current study, we report the binding affinity of terpenoids to one of the host-cell entry routes of SARS-CoV-2, GRP78. All of the 28 terpenoid compounds have comparable binding affinities with the positive control EGCG. At the same time, they are better (lower) than the Pep42 cyclic peptide that is reported to be specific for CS-GRP78 over cancer cells. Moreover, the analyses and the binding free energy, calculated from MM-GBSA, of the best two compounds (GRP78-Oleanolic acid and GRP78-Inonotsulide A) reveal binding strength and stability against GRP78. In essence, terpenoids will have a great impact against the latest variants of SARS-CoV-2, where GRP78 contribution to the recognition of those variants is enhanced, as reported earlier.

Table 4
The Absorption, Distribution, Metabolism, Excretion, and Toxicity (ADMET) properties of the tested terpenoids as calculated using pkCSM webserver.

	Absorbtion			Distribution		Metabolism					Excretion	Toxicity			
Compound name	**Water solubility (log (mol/L))**	**Caco2 permeability**	**Intestinal absorption (human)**	**Fraction unbound (human)**	**BBB permeability**	**CYP1A2 inhibitior**	**CYP2C19 inhibitior**	**CYP2C9 inhibitior**	**CYP2D6 inhibitior**	**CYP3A4 inhibitior**	**Renal OCT2 substrate**	**AMES toxicity**	**hERG I inhibitor**	**hERG II inhibitor**	**Hepatotoxicity**
Inonotsutriol D	−4.32	1.373	100	0.095	−0.275	No	No	No	No	No	No	No	No	No	No
Inonotsutriol B	−4.251	1.2	49.745	0.094	0.569	No	No	No	No	No	No	No	No	No	No
Inonotsuoxodiol A	−4.593	1.384	59.213	0.118	0.543	No	No	No	No	No	No	No	No	No	No
Inonotsuoxide A	−4.546	1.204	100	0.062	0.611	No	No	No	No	No	No	No	No	No	No
Inonotsulide C	−4.456	0.313	60.549	0.084	0.464	No	No	No	No	No	No	No	No	No	No
Inonotsulide A	−4.363	0.438	60.385	0.11	0.535	No	No	No	No	No	No	No	No	No	No
Inonotsudiol A	−4.345	1.276	100	0	−0.336	No	No	No	No	No	No	No	No	No	No
Ergosterol peroxide	−3.642	1.251	80.472	0.139	0.497	No	No	No	No	No	No	No	No	Yes	No
Ergosterol	−4.927	1.255	100	0.025	1.159	No	No	No	No	No	No	No	No	Yes	No
Betulinic acid	−3.151	1.316	100	0.144	0.746	No	No	No	No	No	No	No	No	No	No
Betulin	−4.341	1.331	100	0.127	−0.29	No	No	No	No	No	No	No	No	No	No
3b Hydroxycinnamolide	−2.295	1.211	85.275	0.433	−0.004	No	No	No	No	No	Yes	No	No	No	No
Trametenolic acid	−3.329	1.203	100	0.124	0.735	No	No	No	No	No	No	No	No	No	Yes
Spiroinonotsuoxodiol	−4.248	1.358	62.479	0.101	0.575	No	No	No	No	No	No	No	No	No	No
Oleanolic acid	−3.02	1.252	53.696	0.151	0.747	No	No	No	No	No	No	No	No	No	Yes
Lanosterol	−4.795	1.273	100	0.012	1.176	No	No	No	No	No	No	No	No	Yes	No
Inotodiol	−4.253	1.416	100	0.068	−0.291	No	No	No	No	No	No	No	No	No	No
Inonotusol G	−5.974	1.373	94.283	0	−0.196	No	No	No	No	No	No	No	No	No	No
Inonotusol F	−4.511	1.418	100	0.003	0.678	No	No	No	No	No	No	No	No	No	No
Inonotusol E	−3.74	0.376	63.728	0.25	−0.165	No	No	No	No	No	No	No	No	No	Yes
Inonotusol D	−3.799	0.687	62.548	0.149	−0.198	No	No	No	No	No	No	No	No	No	Yes
Inonotusol C	−3.799	0.687	62.548	0.149	−0.198	No	No	No	No	No	No	No	No	No	Yes
Inonotusol B	−3.957	0.631	64.612	0.308	−0.377	No	No	No	No	No	No	No	No	No	No
Inonotusol A	−3.957	0.631	64.612	0.308	−0.377	No	No	No	No	No	No	No	No	No	No
Inonotusic acid	−5.861	1.755	96.964	0	0.054	Yes	Yes	No	No	No	No	No	No	No	No
Inonotusane C	−4.597	1.251	100	0.026	−0.213	No	No	No	No	No	No	No	No	No	No
Inonotusane B	−4.251	1.2	49.745	0.094	0.569	No	No	No	No	No	No	No	No	No	No
Inonotsutriol E	−4.32	1.373	100	0.095	−0.275	No	No	No	No	No	No	No	No	No	No

Availability of data and material

The docking structures are available upon request from the corresponding author.

Code availability

No codes are involved in this work.

Authors' contributions

W.E. & **A.E.** drafted and revised the manuscript. **A.E.** owns the idea, made the calculations, and drafted the manuscript. **I.I.** performed the after docking MDS, MM-GBSA, and ADMET calculations. All of the authors approved the final version.

Declaration of competing interest

The author declares no competing interest in this work.

Acknowledgments

The researchers wish to extend their sincere gratitude to the Deanship of Scientific Research at the Islamic University of Madinah for the support provided to the Post-Publishing Program 1.

Appendix A. Supplementary data

Supplementary data to this article can be found online at https://doi.org/10.1016/j.compbiomed.2022.105478.

References

[1] A. Khan, S. Hussain, S. Ahmad, M. Suleman, I. Bukhari, T. Khan, F. Rashid, A. K. Azad, M. Waseem, W. Khan, et al., Computational modelling of potentially emerging SARS-CoV-2 spike protein RBDs mutations with higher binding affinity towards ACE2: a structural modelling study, Comput. Biol. Med. 141 (2022) 105163, https://doi.org/10.1016/j.compbiomed.2021.105163.

[2] S. Adem, V. Eyupoglu, I. Sarfraz, A. Rasul, A.F. Zahoor, M. Ali, M. Abdalla, I. M. Ibrahim, A.A. Elfiky, Caffeic acid derivatives (CAFDs) as inhibitors of SARS-CoV-2: CAFDs-based functional foods as a potential alternative approach to combat COVID-19, Phytomedicine 85 (2021) 153310, https://doi.org/10.1016/j.phymed.2020.153310.

[3] I.M. Ibrahim, D.H. Abdelmalek, M.E. Elshahat, A.A. Elfiky, COVID-19 spike-host cell receptor GRP78 binding site prediction, J. Infect. 80 (2020) 554–562, https://doi.org/10.1016/j.jinf.2020.02.026.

[4] X. Huang, W. Dong, A. Milewska, A. Golda, Y. Qi, Q.K. Zhu, W.A. Marasco, R. S. Baric, A.C. Sims, K. Pyrc, et al., Human coronavirus HKU1 spike protein uses O-acetylated sialic acid as an attachment receptor determinant and employs hemagglutinin-esterase protein as a receptor-destroying enzyme, J. Virol. 89 (2015) 7202–7213, https://doi.org/10.1128/JVI.00854-15.

[5] V.S. Raj, H. Mou, S.L. Smits, D.H. Dekkers, M.A. Muller, R. Dijkman, D. Muth, J. A. Demmers, A. Zaki, R.A. Fouchier, et al., Dipeptidyl peptidase 4 is a functional receptor for the emerging human coronavirus-EMC, Nature 495 (2013) 251–254, https://doi.org/10.1038/nature12005.

[6] S. Belouzard, J.K. Millet, B.N. Licitra, G.R. Whittaker, Mechanisms of coronavirus cell entry mediated by the viral spike protein, Viruses 4 (2012) 1011–1033, https://doi.org/10.3390/v4061011.

[7] H. Hofmann, K. Pyrc, L. van der Hoek, M. Geier, B. Berkhout, S. Pohlmann, Human coronavirus NL63 employs the severe acute respiratory syndrome coronavirus receptor for cellular entry, Proc. Natl. Acad. Sci. U. S. A. 102 (2005) 7988–7993, https://doi.org/10.1073/pnas.0409465102.

[8] A. Hasan, B.A. Paray, A. Hussain, F.A. Qadir, F. Attar, F.M. Aziz, M. Sharifi, H. Derakhshankhah, B. Rasti, M. Mehrabi, et al., A review on the cleavage priming of the spike protein on coronavirus by angiotensin-converting enzyme-2 and furin, J. Biomol. Struct. Dyn. (2020) 1–13, https://doi.org/10.1080/07391102.2020.1754293.

[9] A.J. Carlos, D.P. Ha, D.-W. Yeh, R. Van Krieken, P. Gill, K. Machida, A.S. Lee, GRP78 binds SARS-CoV-2 Spike protein and ACE2 and GRP78 depleting antibody blocks viral entry and infection in vitro, bioRxiv 2021 (2021), https://doi.org/10.1101/2021.01.20.427368, 2001.2020.427368.

[10] S. Zhang, K. Amahong, X. Sun, X. Lian, J. Liu, H. Sun, Y. Lou, F. Zhu, Y. Qiu, The miRNA: a small but powerful RNA for COVID-19, Briefings Bioinf. 22 (2021) 1137–1149, https://doi.org/10.1093/bib/bbab062.

[11] O. Omotuyi, O. Olubiyi, O. Nash, E. Afolabi, B. Oyinloye, S. Fatumo, M. Femi-Oyewo, S. Bogoro, SARS-CoV-2 Omicron spike glycoprotein receptor binding domain exhibits super-binder ability with ACE2 but not convalescent monoclonal antibody, Comput. Biol. Med. 142 (2022) 105226, https://doi.org/10.1016/j.compbiomed.2022.105226.

[12] A. Nag, S. Paul, R. Banerjee, R. Kundu, In silico study of some selective phytochemicals against a hypothetical SARS-CoV-2 spike RBD using molecular docking tools, Comput. Biol. Med. 137 (2021) 104818, https://doi.org/10.1016/j.compbiomed.2021.104818.

[13] M.M.H. Sakib, A.A. Nishat, M.T. Islam, M.A. Raihan Uddin, M.S. Iqbal, F.F. Bin Hossen, M.I. Ahmed, M.S. Bashir, T. Hossain, U.S. Tohura, et al., Computational screening of 645 antiviral peptides against the receptor-binding domain of the spike protein in SARS-CoV-2, Comput. Biol. Med. 136 (2021) 104759, https://doi.org/10.1016/j.compbiomed.2021.104759.

[14] A.S. Lee, GRP78 induction in cancer: therapeutic and prognostic implications, Cancer Res. 67 (2007) 3496–3499, https://doi.org/10.1158/0008-5472.CAN-07-0325.

[15] J. Li, A.S. Lee, Stress induction of GRP78/BiP and its role in cancer, Curr. Mol. Med. 6 (2006) 45–54, https://doi.org/10.2174/156652406775574523.

[16] K.T. Pfaffenbach, A.S. Lee, The critical role of GRP78 in physiologic and pathologic stress, Curr. Opin. Cell Biol. 23 (2011) 150–156, https://doi.org/10.1016/j.ceb.2010.09.007.

[17] I.M. Ibrahim, D.H. Abdelmalek, A.A. Elfiky, GRP78: a cell's response to stress, Life Sci. 226 (2019) 156–163, https://doi.org/10.1016/j.lfs.2019.04.022.

[18] L.H. Zhang, X. Zhang, Roles of GRP78 in physiology and cancer, J. Cell. Biochem. 110 (2010) 1299–1305, https://doi.org/10.1002/jcb.22679.

[19] M. Gonzalez–Gronow, M.A. Selim, J. Papalas, S.V. Pizzo, GRP78: a multifunctional receptor on the cell surface, Antioxidants Redox Signal. 11 (2009) 2299–2306.

[20] A.A. Al-Hashimi, J. Rak, R.C. Austin, Cell surface GRP78: a novel regulator of tissue factor procoagulant activity, in: Cell Surface GRP78, a New Paradigm in Signal Transduction Biology, Elsevier, 2018, pp. 63–85.

[21] S. Pujhari, V.M. Macias, R.H. Nissly, M. Nomura, S.V. Kuchipudi, J.L. Rasgon, Heat shock protein 70 (Hsp70) is involved in the Zika virus cellular infection process, bioRxiv (2017) 135350.

[22] M. Nain, S. Mukherjee, S.P. Karmakar, A.W. Paton, J.C. Paton, M. Abdin, A. Basu, M. Kalia, S. Vrati, GRP78 is an important host-factor for Japanese encephalitis virus entry and replication in mammalian cells, J. Virol. (2017). JVI. 02274-02216.

[23] T. Chen, S. Xu, Chronic exposure of cisplatin induces GRP78 expression in ovarian cancer, in: Proceedings of the Proceedings of the, International Conference on Biomedical and Bioinformatics Engineering, 2017, pp. 35–38, 2017 4th.

[24] U.K. Misra, M. Gonzalez-Gronow, G. Gawdi, S.V. Pizzo, The role of MTJ-1 in cell surface translocation of GRP78, a receptor for alpha 2-macroglobulin-dependent signaling, J. Immunol. 174 (2005) 2092–2097, https://doi.org/10.4049/jimmunol.174.4.2092, 1950, Baltimore, Md.

[25] I.M. Ibrahim, D.H. Abdelmalek, A.A. Elfiky, GRP78: a cell's response to stress, Life Sci. 226 (2019) 156–163, https://doi.org/10.1016/j.lfs.2019.04.022.

[26] A.A. Elfiky, Human papillomavirus E6: host cell receptor, GRP78, binding site prediction, J. Med. Virol. (2020) n/a, https://doi.org/10.1002/jmv.25737.

[27] A. Nassar, I.M. Ibrahim, F.G. Amin, M. Magdy, A.M. Elgharib, E.B. Azzam, F. Nasser, K. Yousry, I.M. Shamkh, S.M. Mahdy, et al., A review of human coronaviruses' receptors: the host-cell targets for the crown bearing viruses, Molecules 26 (2021) 6455.

[28] A.M. Elgohary, A.A. Elfiky, K.G.R.P.78 Barakat, A possible relationship of COVID-19 and the mucormycosis; in silico perspective, Comput. Biol. Med. 139 (2021) 104956, https://doi.org/10.1016/j.compbiomed.2021.104956.

[29] R. Sabirli, A. Koseler, T. Goren, I. Turkcuer, O. Kurt, High GRP78 levels in Covid-19 infection: a case-control study, Life Sci. 265 (2021) 118781, https://doi.org/10.1016/j.lfs.2020.118781.

[30] J. Fu, C. Wei, J. He, L. Zhang, J. Zhou, K.S. Balaji, S. Shen, J. Peng, A. Sharma, J. Fu, Evaluation and characterization of HSPA5 (GRP78) expression profiles in normal individuals and cancer patients with COVID-19, Int. J. Biol. Sci. 17 (2021) 897–910, https://doi.org/10.7150/ijbs.54055.

[31] V. Roviello, G.N. Roviello, Less COVID-19 deaths in southern and insular Italy explained by forest bathing, Mediterranean environment, and antiviral plant volatile organic compounds, Environ. Chem. Lett. (2021) 1–11, https://doi.org/10.1007/s10311-021-01309-5.

[32] C. Vicidomini, V. Roviello, G.N. Roviello, Silico investigation on the interaction of chiral phytochemicals from opuntia ficus-indica with SARS-CoV-2 mpro, Symmetry 13 (2021) 1041.

[33] G.A. Gyebi, A.A. Elfiky, O.M. Ogunyemi, I.M. Ibrahim, A.P. Adegunloye, J. O. Adebayo, C.O. Olaiya, J.O. Ocheje, M.M. Fabusiwa, Structure-based virtual screening suggests inhibitors of 3-Chymotrypsin-Like Protease of SARS-CoV-2 from Vernonia amygdalina and Occinum gratissimum, Comput. Biol. Med. 136 (2021) 104671, https://doi.org/10.1016/j.compbiomed.2021.104671.

[34] A. Palmeira, E. Sousa, A. Köseler, R. Sabirli, T. Gören, İ. Türkçüer, Ö. Kurt, M. M. Pinto, M.H. Vasconcelos, Preliminary virtual screening studies to identify GRP78 inhibitors which may interfere with SARS-CoV-2 infection, Pharmaceuticals 13 (2020) 132.

[35] A.A. Elfiky, Natural products may interfere with SARS-CoV-2 attachment to the host cell, J. Biomol. Struct. Dyn. 39 (2021) 3194–3203, https://doi.org/10.1080/07391102.2020.1761881.

[36] K.O. Suk-Kyung, Y.U.N. Soo-Jeung, P. Sun-Young, P.Y.O. Myoung-Yun, Immunomodulating effects of Chaga mushroom (Inonotus obliquus) in OVA-sensitized balb/c mice, 춘계총회 및 학술대회 (2010), 156-156.

[37] A.H.N. Sung-Hoon, C. Eun-Jung, J. Jong-Hyun, J. Su-Min, K. So-Young, B.A. E. Myung-Ae, Summarized report of ADME/tox screening data in KRICT, 춘계총회 및 학술대회 (2010), 2009, 244-244.

[38] W.E. Basal, Abdo, J. Eid, Chaga medicinal mushroom Inonotus obliquus (agaricomycetes) terpenoids may interfere with SARS-CoV-2 spike protein recognition of the host cell: a molecular docking study, Int. J. Med. Mushrooms 23 (3) (2021) 1–14, https://doi.org/10.1615/IntJMedMushrooms.2021037942.
[39] A. Sonousi, H.A. Mahran, I.M. Ibrahim, M.N. Ibrahim, A.A. Elfiky, W.M. Elshemey, Novel adenosine derivatives against SARS-CoV-2 RNA-dependent RNA polymerase: an in silico perspective, Pharmacol. Rep. 73 (2021) 1754–1764, https://doi.org/10.1007/s43440-021-00300-9.
[40] I.M. Ibrahim, A.A. Elfiky, A.M. Elgohary, Recognition through GRP78 is enhanced in the UK, South African, and Brazilian variants of SARS-CoV-2; an in silico perspective, Biochem. Biophys. Res. Commun. 562 (2021) 89–93, https://doi.org/10.1016/j.bbrc.2021.05.058.
[41] A.A. Elfiky, I.M. Ibrahim, F.G. Amin, A.M. Ismail, W.M. Elshemey, COVID-19 and cell stress, Adv. Exp. Med. Biol. 1318 (2021) 169–178, https://doi.org/10.1007/978-3-030-63761-3_10.
[42] B.R. Miller 3rd, T.D. McGee Jr., J.M. Swails, N. Homeyer, H. Gohlke, A.E. Roitberg, MMPBSA.py: an efficient Program for end-state free energy calculations, J. Chem. Theor. Comput. 8 (2012) 3314–3321, https://doi.org/10.1021/ct300418h.
[43] S. Kim, P.A. Thiessen, E.E. Bolton, J. Chen, G. Fu, A. Gindulyte, L. Han, J. He, S. He, B.A. Shoemaker, PubChem substance and compound databases, Nucleic Acids Res. 44 (2015) D1202–D1213.
[44] G.M. Morris, R. Huey, W. Lindstrom, M.F. Sanner, R.K. Belew, D.S. Goodsell, A.J. AutoDock4 Olson, AutoDockTools4, Automated docking with selective receptor flexibility, J. Comput. Chem. 30 (2009) 2785–2791, https://doi.org/10.1002/jcc.21256.
[45] M.D. Hanwell, D.E. Curtis, D.C. Lonie, T. Vandermeersch, E. Zurek, G.R. Hutchison, Avogadro: an advanced semantic chemical editor, visualization, and analysis platform, J. Cheminf. 4 (2012) 17, https://doi.org/10.1186/1758-2946-4-17.
[46] A.K. Rappe, C.J. Casewit, K.S. Colwell, W.A. Goddard, W.M. Skiff, UFF, a full periodic table force field for molecular mechanics and molecular dynamics simulations, J. Am. Chem. Soc. 114 (2002) 10024–10035, https://doi.org/10.1021/ja00051a040.
[47] J. Yang, R. Yan, A. Roy, D. Xu, J. Poisson, Y. Zhang, The I-TASSER Suite: protein structure and function prediction, Nat. Methods 12 (2015) 7–8, https://doi.org/10.1038/nmeth.3213.
[48] Y. Kim, A.M. Lillo, S.C. Steiniger, Y. Liu, C. Ballatore, A. Anichini, R. Mortarini, G. F. Kaufmann, B. Zhou, B. Felding-Habermann, Targeting heat shock proteins on cancer cells: selection, characterization, and cell-penetrating properties of a peptidic GRP78 ligand, Biochemistry 45 (2006) 9434–9444.
[49] J.C. Phillips, R. Braun, W. Wang, J. Gumbart, E. Tajkhorshid, E. Villa, C. Chipot, R. D. Skeel, L. Kale, K. Schulten, Scalable molecular dynamics with NAMD, J. Comput. Chem. 26 (2005) 1781–1802, https://doi.org/10.1002/jcc.20289.
[50] J. Huang, A.D. MacKerell Jr., CHARMM36 all-atom additive protein force field: validation based on comparison to NMR data, J. Comput. Chem. 34 (2013) 2135–2145, https://doi.org/10.1002/jcc.23354.
[51] Schrödinger Release 2017-1, Maestro, Schrödinger, LLC, New York, NY, 2017. Available online: (accessed on.
[52] J. Yang, M. Nune, Y. Zong, L. Zhou, Q. Liu, Close and allosteric opening of the polypeptide-binding site in a human Hsp70 chaperone BiP, Structure 23 (2015) 2191–2203, https://doi.org/10.1016/j.str.2015.10.012.
[53] J. Yang, Y. Zong, J. Su, H. Li, H. Zhu, L. Columbus, L. Zhou, Q. Liu, Conformation transitions of the polypeptide-binding pocket support an active substrate release from Hsp70s, Nat. Commun. 8 (2017) 1201, https://doi.org/10.1038/s41467-017-01310-z.
[54] 2.4.1, P.V. The PyMOL Molecular Graphics System, Version 2.4.1 Schrödinger, LLC. Available online: (accessed on).
[55] E.F. Pettersen, T.D. Goddard, C.C. Huang, G.S. Couch, D.M. Greenblatt, E.C. Meng, T.E. Ferrin, UCSF Chimera—a visualization system for exploratory research and analysis, J. Comput. Chem. 25 (2004) 1605–1612.
[56] O. Trott, A.J. Olson, AutoDock Vina, Improving the speed and accuracy of docking with a new scoring function, efficient optimization, and multithreading, J. Comput. Chem. 31 (2010) 455–461, https://doi.org/10.1002/jcc.21334.
[57] A.A. Elfiky, A.M. Baghdady, S.A. Ali, M.I. Ahmed, GRP78 targeting: hitting two birds with a stone, Life Sci. 260 (2020) 118317, https://doi.org/10.1016/j.lfs.2020.118317.
[58] M.A. Rauf, S. Zubair, A. Azhar, Ligand docking and binding site analysis with pymol and autodock/vina, Int. J. Basic Appl. Sci. 4 (2015) 168.
[59] S. Genheden, U. Ryde, The MM/PBSA and MM/GBSA methods to estimate ligand-binding affinities, Expet Opin. Drug Discov. 10 (2015) 449–461, https://doi.org/10.1517/17460441.2015.1032936.
[60] W. Xue, F. Yang, P. Wang, G. Zheng, Y. Chen, X. Yao, F. Zhu, what contributes to serotonin-norepinephrine reuptake inhibitors' dual-targeting mechanism? The key role of transmembrane domain 6 in human serotonin and norepinephrine transporters revealed by molecular dynamics simulation, ACS chemical neuroscience 9 (2018) 1128–1140, https://doi.org/10.1021/acschemneuro.7b00490.
[61] T. Tuccinardi, What is the current value of MM/PBSA and MM/GBSA methods in drug discovery? Expet Opin. Drug Discov. 16 (2021) 1233–1237, https://doi.org/10.1080/17460441.2021.1942836.
[62] D.E. Pires, T.L. Blundell, D.B. Ascher, pkCSM: Predicting small-molecule pharmacokinetic and toxicity properties using graph-based signatures, J. Med. Chem. 58 (2015) 4066–4072, https://doi.org/10.1021/acs.jmedchem.5b00104.
[63] K. Gurusinghe, A. Mishra, S. Mishra, Glucose-regulated protein 78 substrate-binding domain alters its conformation upon EGCG inhibitor binding to nucleotide-binding domain: molecular dynamics studies, Sci. Rep. 8 (2018) 5487, https://doi.org/10.1038/s41598-018-22905-6.
[64] J.I. Eid, B. Das, M.M. Al-Tuwaijri, W.T. Basal, Targeting SARS-CoV-2 with Chaga mushroom: an in silico study toward developing a natural antiviral compound, Food Sci. Nutr. 9 (2021) 6513–6523, https://doi.org/10.1002/fsn3.2576.
[65] Y. Kim, A.M. Lillo, S.C. Steiniger, Y. Liu, C. Ballatore, A. Anichini, R. Mortarini, G. F. Kaufmann, B. Zhou, B. Felding-Habermann, et al., Targeting heat shock proteins on cancer cells: selection, characterization, and cell-penetrating properties of a peptidic GRP78 ligand, Biochemistry 45 (2006) 9434–9444, https://doi.org/10.1021/bi060264j.
[66] Y. Yoneda, S.C. Steiniger, K. Capkova, J.M. Mee, Y. Liu, G.F. Kaufmann, K. D. Janda, A cell-penetrating peptidic GRP78 ligand for tumor cell-specific prodrug therapy, Bioorg. Med. Chem. Lett 18 (2008) 1632–1636, https://doi.org/10.1016/j.bmcl.2008.01.060.
[67] C.A. Lipinski, Lead- and drug-like compounds: the rule-of-five revolution, Drug Discov. Today Technologies 1 (2004) 337–341, https://doi.org/10.1016/j.ddtec.2004.11.007.
[68] A.A. Elfiky, I.M. Ibrahim, Host-cell recognition through GRP78 is enhanced in the new UK variant of SARS-CoV-2, in silico, J. Infect. 82 (2021) 186–230, https://doi.org/10.1016/j.jinf.2021.01.015.
[69] A. Elfiky, I.M. Ibrahim, A.M. Elgohary, Host-cell recognition through GRP78 is enhanced in the new variants of SARS-CoV-2; in silico perspective, Biochem. Biophys. Res. Commun. 562 (2021) 89–93.
[70] Elfiky, A.A.; Ibrahim, I.M. Host-cell recognition through Cs-GRP78 is enhanced in the new Omicron variant of SARS-CoV-2, in silico structural point of view. J. Infect., doi:10.1016/j.jinf.2022.01.019.
[71] I. Khater, A. Nassar, SARS-CoV-2 variant surge and vaccine breakthrough infection: a computational analysis, Inform. Med. Unlocked 29 (2022) 100873, https://doi.org/10.1016/j.imu.2022.100873.